# Thermodynamics and the hydrophobic effect in a core-softened model and comparison with experiments

Matej Huš and Tomaz Urbic*

*University of Ljubljana, Department of Chemistry and Chemical Technology, Chair of Physical Chemistry, Aškerčeva 5, SI-1000 Ljubljana, Slovenia*

(Received 19 February 2014; revised manuscript received 23 April 2014; published 14 August 2014)

A simple and computationally inexpensive core-softened model, originally proposed by Franzese [G. Franzese, J. Mol. Liq. **136**, 267 (2007)], was adopted to show that it exhibits properties of waterlike fluid and hydrophobic effect. The potential used between particles is spherically symmetric with two characteristic lengths. Thermodynamics of nonpolar solvation were modeled as an insertion of a modified Lennard-Jones particle. It was investigated how the anomalous predictions of the model as well as the nonpolar solvation compare with the experimental data for water anomalies and the temperature dependence of noble gases hydration. It was shown that the model qualitatively follows the same trends as water. The model is able to reproduce waterlike anomalous properties (density maximum, heat capacity minimum, isothermal compressibility, etc.) and hydrophobic effect (minimum solubility for nonpolar solutes near ambient conditions, increased solubility of larger noble gases, etc.). It is argued that the model yields similar results as more complex and computationally expensive models.

DOI: 10.1103/PhysRevE.90.022115 PACS number(s): 61.20.Ja, 65.20.De, 34.20.Gj

## I. INTRODUCTION

Water is the most abundant and, arguably, the most important fluid on Earth. It influences every aspect of our lives, as it drives the biological processes, serves as a universal solvent, shapes the climate because of its high heat capacity in fluid state and high greenhouse potential in gaseous form, and transforms the Earth's surface through erosion and weathering. In the biosphere, water accounts for more than half of the weight of living cells. Industrially, it is used as a coolant, solvent, and reactant. Unwanted effects of water include corrosion, mobilization of harmful species, and dilution and redistribution of toxins [1,2].

Somewhat ironically, water is also one of the most unusual liquids [1–5]. It is notable for having a very complex phase diagram with many anomalies, such as the negative slope of liquid-solid boundary; in other words, ice melts under pressure. Related to this is the other well-known anomaly, namely the greater density of water as compared to ice and a temperature range (0–3.984 °C at room pressure, and down to −40 °C when supercooled) where the density of water actually increases with warming. Besides these commonly known and widely taught characteristics, water possesses many other anomalous properties. Among them one should note unusually high boiling and melting points, surface tension, and viscosity when compared to simple liquids, presence of minima in the isobaric heat capacity and isothermal compressibility, diffusion coefficient maximum [5,6], and a putative [7] phase transition between low-density fluid and high-density fluid in the supercooled region [8–11]. Liquid-liquid phase transition has also been found in a few other substances, such as silica [8,12,13], $BeF_2$ [14], and some liquid metals.

The exact mechanism of water anomalies has been extensively researched [15–19] and remains a matter of speculation [7,20–24]. It is known, however, that strong and heavily angular-dependent interactions, known as hydrogen bonds, play a vital role. They introduce a competition between the orientational order that favors low-density tetrahedral coordination and the configurational order that favors denser coordinations [25–27]. At lower temperatures, the orientational contribution is dominant, while at higher temperatures the reverse is true. In the region most important for life, i.e., at physiological conditions, the effects are of comparable magnitude.

To simulate angular-dependent interactions, it is necessary to forgo an isotropic potential or spherical particles altogether. One way to do the former is to use spherical particles that interact isotropically and attach a specified number of arms to each, allowing for orientationally dependent interactions, as in the Mercedes-Benz model [28–32]. Alternatively, one can construct point charge models (for instance TIP5P [4]), where hydrogen and oxygen atoms and electron pairs are modeled explicitly. Such models may even include polarizability effects (such as the Gaussian charge polarizable model (GCPM) [33]). In each case, however, the computational cost scales quadratically with the number of particles used.

It is possible to construct isotropic potentials that bridge this gap, as shown by Stillinger *et al.* [34] and Garde *et al.* [35]. Formally speaking, competition between the orientational and translational order manifests as two characteristic lengths of separation for the particles involved. Averaging the interaction in angular-dependent water models yields a core-softened potential in the first-order approximation [36,37]. Not surprisingly, several such isotropic core-softened potentials have been developed over time, including (repulsive) shoulder potentials [11], ramp potentials [38,39], Jagla potential [40–43], honeycomb potential [44], Lennard-Jones-Gaussian potentials [45,46], and continuous shouldered well (CSW) potential [47]. They were first used to account for the isostructural solid-solid phase transition in a lattice gas system [48,49], but their applicability in describing waterlike fluids and liquid metals was soon noticed [50–57]. Isotropic potentials have either been calculated from reverse Monte Carlo (MC)

*tomaz.urbic@fkkt.uni-lj.si

 

simulations [58] or proposed arbitrarily. For many of these models, several waterlike properties have been unearthed, from solvent anomalies to solvation mechanism [59,60] and small solute aggregation [61,62]. It has also been shown that all these models invariably suffer from some transferability issues. In approximating angular-dependent interactions with isotropic potentials, approximations that effect certain artifacts are introduced. Even when using isotropic potentials derived from simulation pair correlation functions, models will not be able to reproduce all physical properties without allowing the potential to change according to the state of the system [63,64]. This limits the predictive power of such models.

In this paper, it was shown how the CSW potential, originally proposed by Franzese [47], is able to reproduce similar anomalies to those found in pure water [20,65–67]. Furthermore, solvation of various nonpolar solutes is investigated. Using this model, it is possible to obtain behavior, collectively known in water as the hydrophobic effect [61,68–70]. The hydrophobic effect usually manifests as a large free energy for transfer of a small nonpolar solute into water, a large negative entropy of transfer at room conditions, and a strong temperature dependence of entropy and enthalpy of transfer [70,71] due to ordering of water molecules around the solute [58]. For larger solutes, the solvation mechanism changes and the free energy scales with the surface [59,61,62,72]. The hydrophobic effect and the penetration of the solvent particles between the hydrophobic solutes are also implicated in cold denaturation of proteins [73–78].

This paper is organized as follows. After detailing the model layout and a presentation of simulation details, we first present parametrization of the model so that we can directly compare results with experiment. Anomalous properties of water are then contrasted with the pure CSW solvent, showing matching trends. Differences between the model and water and the limitations of the model are discussed. In the second part, we deal with the solvation of nonpolar solutes and the hydrophobic effect. We compare experimental data on the solvation of a hydrophobic particle (argon) with the results from the model. Lastly, we show that the model also accounts for the differences in size and interaction strength of the solute particles. Various Lennard-Jones (LJ) particles are constructed according to experimental parameters of noble gases and methane. Hydration of noble gases and methane under high pressure is compared to the model results for the solvation of the aforementioned solutes.

## II. MODEL

Solvent molecules are represented as soft-core spherical particles, interacting through the pairwise potential function, originally proposed by Franzese [47]

$$U(r) = \frac{U_R}{1+\exp(\Delta(r-R_R)/a)} - U_A \exp\left(-\frac{(r-R_A)^2}{2\delta_A^2}\right) + U_A\left(\frac{a}{r}\right)^{24}. \quad (1)$$

Distance dependence of the potential is shown in Fig. 1(b). The potential can be decomposed into three parts: a steep repulsive wall, a soft repulsive shoulder of height $U_R$, and an attractive Gaussian well of depth $U_A$ and width $2\delta_A\sqrt{2\ln 2}$. $R_R$ and $R_A$ are the repulsive average radius and the location of the potential minimum, respectively, with $a$ determining the diameter of particles. It is possible to modify the steepness of the repulsive shoulder by varying the parameter $\Delta$. As this paper represents a continuation of our previous work [67,79,80], we opted to keep the potential parameters unchanged, essentially using the original values from Refs. [47,65,66]: $U_R/U_A = 2$, $R_R/a = 1.6$, $R_A/a = 2$, $(\delta_A/a)^2 = 0.1$, $\Delta = 15$.

Interactions between the hydrophobic molecules were modeled with a Lennard-Jones-like potential. To avoid unwanted soft-core effects due to different steepness of the impenetrable potential wall while maintaining the location and depth of the Lennard-Jones minimum, we propose the following LJ-like potential [79]:

$$U_{\mathrm{LJ}} = \frac{4}{3}\times 2^{\frac{2}{3}}\epsilon_{\mathrm{LJ}}\left[\left(\frac{\sigma_{\mathrm{LJ}}}{r}\right)^{24} - \left(\frac{\sigma_{\mathrm{LJ}}}{r}\right)^{6}\right]. \quad (2)$$

Solute-solvent interactions are modeled with the aforementioned LJ-like potential with different parameters. We use Lorentz-Berthelot [81,82] mixing rules:

$$\epsilon_{\mathrm{mix}} = \sqrt{\epsilon_{\mathrm{LJ}}U_A} \quad (3)$$

$$\sigma_{\mathrm{mix}} = \frac{\sigma_{\mathrm{LJ}}+a}{2}, \quad (4)$$

where $\sigma_{\mathrm{LJ}}$ represents the varying diameter of the apolar solute, while $\epsilon_{\mathrm{LJ}} = 0.10$ remained fixed to approximate a typical weakly interacting nonpolar solute, unless stated otherwise. However, as $\sigma_{\mathrm{mix}}$ increases, the width of the attraction well would grow unreasonably large with this convention. To compensate for this, we use the shifted LJ-like potential above $\sigma_{\mathrm{mix}} > \sigma_{\mathrm{tr}} = 1.0$. Using

$$U_{\mathrm{mix}} = \begin{cases} \infty; & \text{for } r < \sigma_{\mathrm{mix}} - \sigma_{\mathrm{tr}} \\ \frac{4}{3}\cdot 2^{\frac{2}{3}}\epsilon_{\mathrm{mix}}\left[\left(\frac{\sigma_{\mathrm{tr}}}{r-(\sigma_{\mathrm{mix}}-\sigma_{\mathrm{tr}})}\right)^{24} - \left(\frac{\sigma_{\mathrm{tr}}}{r-(\sigma_{\mathrm{mix}}-\sigma_{\mathrm{tr}})}\right)^{6}\right]; & \text{for } r \geqslant \sigma_{\mathrm{mix}} - \sigma_{\mathrm{tr}} \end{cases} \quad (5)$$

we effectively shift the position of the attraction well while keeping its width characteristic of $\sigma_{\mathrm{tr}} = 1.0$ [see Fig. 1(b)].

## III. METHODS

The system was studied using Monte Carlo simulations in the NPT ensemble [83]. A cubic box using the minimum image convention consisted of 300 particles when dealing with solutes $\sigma_{\mathrm{LJ}} < 2.0$ and 600 particles otherwise. A few simulations with twice as many particles were carried out to ensure that finite-size effects do not introduce any artifacts.

Equilibration of the system took $10^5$ cycles with one cycle being an attempted move of each particle and an attempted change of volume. After equilibration, the statistics were sampled across ten runs of $10^5$ cycles to ensure sufficient sampling of the phase space and obtain the averaged results. To

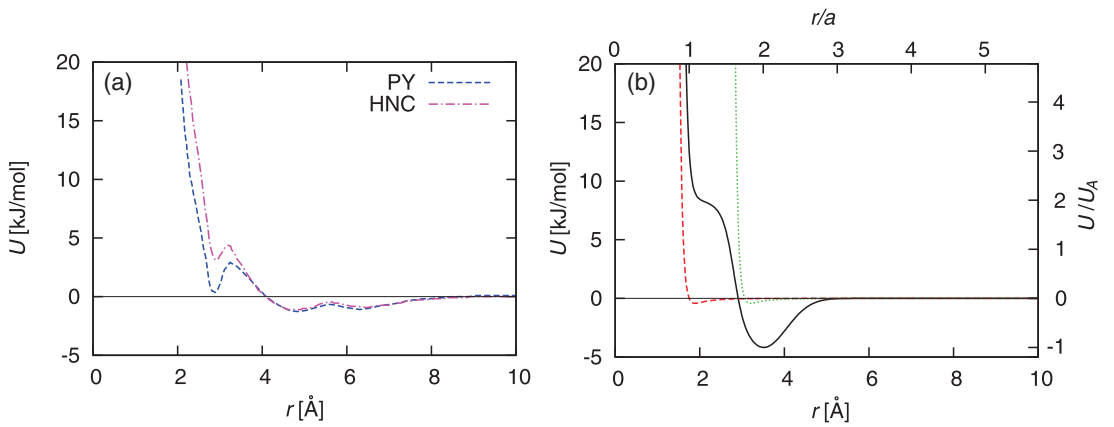


FIG. 1. (Color online) Two characteristic lengths in a pair potential suffice to reproduce the behavior of water. (a) Inversion of the experimental oxygen-oxygen radial distribution function [36,37] yields an effective pair potential. Competition between orientational order due to strong angular-dependent interactions (hydrogen bonding) and translational order manifests as two characteristic lengths in a potential. (b) The soft-core potential (solid line) used in our simulations (CSW) can be thought of as a first-order approximation of the experimental potential. Also, a modified Lennard-Jones potential for solute-solvent interaction for two particle sizes (dashed and dotted lines) is shown, which is used to simulate hydrophobic particles.

evaluate pair distribution functions, however, simulation runs had to be extended to $4 \times 10^6$ cycles to sufficiently minimize statistical noise.

Volume and enthalpy were computed as the averages over the simulation runs and averaged over all independent runs to calculate the standard deviation. Thermodynamic properties of a solvation process were computed with three distinct methods. For small particles ($\sigma_{\mathrm{LJ}} < 2.0$), Widom's particle insertion method [84] proved to be the most efficient way of calculation. At each cycle, a ghost solute particle is placed randomly into the box and not allowed to interact with the solvent particles. We then calculate the hypothetical interaction of the ghost particle with the solvent, and its weighted average. Thermodynamic quantities describing the solvation (free energy $\Delta G$, enthalpy $\Delta H$, entropy $\Delta S$, and heat capacity $\Delta c_p$) and change in volume ($\Delta V$) follow from [85]:

$$\Delta G = -\beta^{-1} \ln \left[ \langle V \rangle_N^{-1} \langle V \exp(-\beta U) \rangle_N \right] \tag{6}$$

$$\Delta H = \frac{\langle H_{N+1} \exp(-\beta U) \rangle_N}{\langle \exp(-\beta U) \rangle_N} - \langle H_N \rangle_N \tag{7}$$

$$T \Delta S = \Delta H - \Delta G \tag{8}$$

$$k_b T^2 \Delta c_p = \frac{\left\langle H_{N+1}^2 \exp(-\beta U) \right\rangle_N}{\langle \exp(-\beta U) \rangle_N} - \frac{\langle H_{N+1} \exp(-\beta U) \rangle_N^2}{\langle \exp(-\beta U) \rangle_N^2} - \left\langle H_N^2 \right\rangle_N + \langle H_N \rangle_N^2 \tag{9}$$

$$\Delta V = \frac{\langle V \exp(-\beta U) \rangle_N}{\langle \exp(-\beta U) \rangle_N} - \langle V \rangle_N, \tag{10}$$

where $\beta = (k_b T)^{-1}$. Angle brackets $\langle \ldots \rangle_N$ denote averages throughout the run over all insertions. $U$ is the interaction of the ghost particle with the system and $H_{N+1}$ represents the enthalpy of the system with the ghost particle. $\langle H_N \rangle_N$ and $\langle H_N^2 \rangle_N$ stand for the average enthalpy and the average of squared enthalpy, respectively, of the system without the ghost particle.

For large particles, the probability of a successful insertion decreases exponentially. Therefore, the free energy perturbation (FEP) [86] method was used. A solute of size $\sigma_A$ was fixed at the center of the simulation box and allowed to interact with solvent particles. Once each cycle, total interaction of the central particle with the solvent particles was calculated, first using its actual size $\sigma_A$ and then the would-be interaction, were the particle of size $\sigma_B$, yielding $U_A$ and $U_B$, respectively. The free energy difference for increasing the size of the solute particle from $\sigma_A$ to $\sigma_B$ is obtained from the weighted average as

$$\Delta G = -k_B T \ln \left\langle \exp\left( -\frac{U_B - U_A}{k_B T} \right) \right\rangle. \tag{11}$$

Starting from a known value of the free energy of solvation from Widom's insertion method, one can calculate the energy of solvation for successively larger solutes, provided that the step of the diameter increase is not too large to significantly violate the reversibility condition.

To circumvent the tedious process of successively increasing the solute size, thermodynamic integration (TI) is employed instead for very large particles ($\sigma_{\mathrm{LJ}} > 5.0$). A solute particle is fixed at the center of the simulation box. Its interaction with the solvent particles is slowly turned on with varying the parameter $\lambda$ from 0–1.

$$U_{\mathrm{LJ}} = \frac{4}{3} \times 2^{\frac{2}{3}} \epsilon_{\mathrm{LJ}} \lambda^n \left[ \frac{1}{\left( \alpha (1-\lambda)^m + \left( \frac{r}{\sigma_{\mathrm{LJ}}} \right)^{12} \right)^2} - \frac{1}{\left( \alpha (1-\lambda)^m + \left( \frac{r}{\sigma_{\mathrm{LJ}}} \right)^{6} \right)^2} \right]. \tag{12}$$

Ancillary parameters were set to $m = n = 2$ and $\alpha = 0.5$ for better convergence.

In each simulation, the derivative of the solute-solvent potential with respect to $\lambda$ and the volume are averaged. The free energy for transfer of a solute particle into the solution is

given by

$$\Delta G = \int_{\lambda=0}^{\lambda=1} \frac{\partial U_{\mathrm{LJ}}}{\partial \lambda}\, d\lambda + \ln \frac{V_{(\lambda=1.0)}}{V_{(\lambda=0.0)}}. \tag{13}$$

In both approaches, enthalpy of solvation was calculated via the Gibbs-Helmholtz equation, yielding entropy in the process, as well.

$$\left(\frac{\partial \frac{\Delta G}{T}}{\partial T}\right)_p = -\frac{\Delta H}{T^2} \tag{14}$$

$$T\Delta S = \Delta H - \Delta G. \tag{15}$$

For a few solute sizes, all methods were carried out as to ensure that they yield quantitatively matching results [cf. Fig. 6(c) with juxtaposed results from all methods].

## IV. RESULTS AND DISCUSSION

### A. Transferability

The results of simulations are reported in dimensionless reduced units, relative to the solvent diameter and the depth of its attractive well, as $T^* = k_B T/U_A$, $\rho^* = \rho a^3$, and $p^* = pa^3/U_A$. The model was also parametrized. Setting $U_A =$ 4200 J mol$^{-1}$ and $a = 1.75$ Å, it is possible to translate reduced units into physical units. As the potential features only two variable parameters, certain tradeoffs were necessary. $U_A$ and $a$ were chosen in such a way to try to reproduce the density of the liquid phase as close as possible, while keeping other quantities in the correct order of magnitude. We should also accentuate that values of parameters have no direct connection to hydrogen bond strength and hydrogen bond length as they represent averaged effective potential. Therefore we use two sets of axes on our plots, one corresponding to the reduced units and the other one to physical units.

Despite known shortcomings of isotropic potentials [63,64] stemming from the fact that they remain fixed as the thermodynamic state of the system changes, we decided not to change the model parameters with the state of system. Our aim was to show that a simplified model can reproduce anomalies and, more importantly, that there is a parametrization that causes them to manifest in the range where water is liquid.

### B. Structure

Water molecules can form at most four hydrogen bonds with the neighboring molecules, two donor and two acceptor bonds. Hydrogen bonds have long been thought to be the determining force for highly ordered structure of water [1]. The strength of a single hydrogen bond strongly varies with local environment [87] and they are generally stronger than van der Waals interactions. Nevertheless, they are the competing force of non-negligible magnitude [88], favoring a less ordered configuration with a higher coordination number. This competition between the low-density orientational order and high-density translational order is believed to account for many anomalous properties of water and can be observed experimentally.

Oxygen-oxygen radial distribution function for liquid water at room conditions was obtained from neutron diffraction experiments by Soper and Phillips [89]. Using the Ornstein-Zernike integral equation, the effective, orientationally averaged water-water potential was obtained from these data in Percus-Yevick and hypernetted chain approximation [36,37]. Of particular interest is the shape of the potential function, revealing two characteristic distances [see Fig. 1(a)]. The first, shallower minimum corresponds to the translational order and the second, global minimum to the orientational. As the CSW is an isotropic potential, this waterlike behavior is reproduced by two characteristic lengths [see Fig. 1(b)]. Such soft-core potentials can therefore be viewed as a first-order approximation of the experimental potential, as proved by the spherically symmetric HGS (named after authors' initials Head-Gordon, Stillinger [36]) potential calculated using reverse MC simulation and fit to that of simple point charge (SPC) water [90]. One should note that effective potential is not constant at all phase points, but depends on density and temperature. This is an additional approximation in all calculations making exact comparison with experiment difficult. The potential used in this work is therefore a less veracious rendition of the water effective potential because we do not seek to reproduce the water anomalies *per se*, but

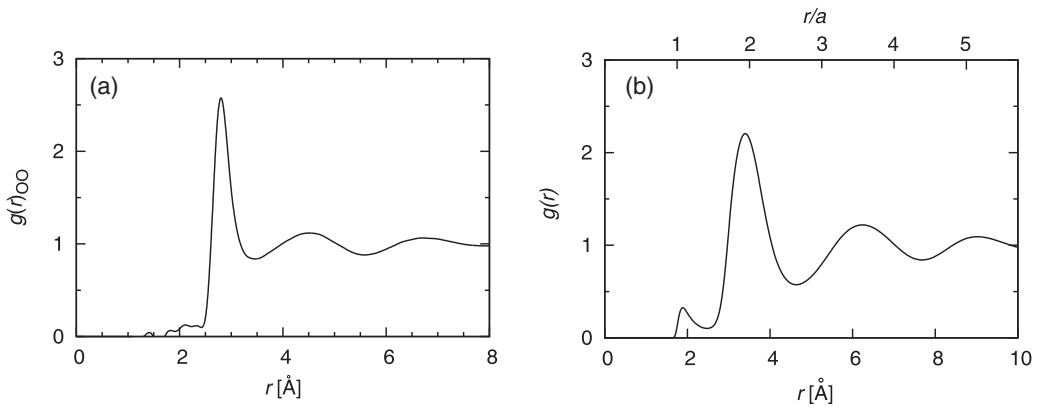


FIG. 2. (a) Oxygen-oxygen radial distribution function in liquid water at 25 °C and 1 atm from neutron scattering experiment [91]. (b) Radial distribution function from a simulation in the CSW solvent slightly above the melting point and at subcritical pressure, $T^* = 0.6$ and $p^* = 0.0002$, corresponding to 30 °C and 2.6 atm.

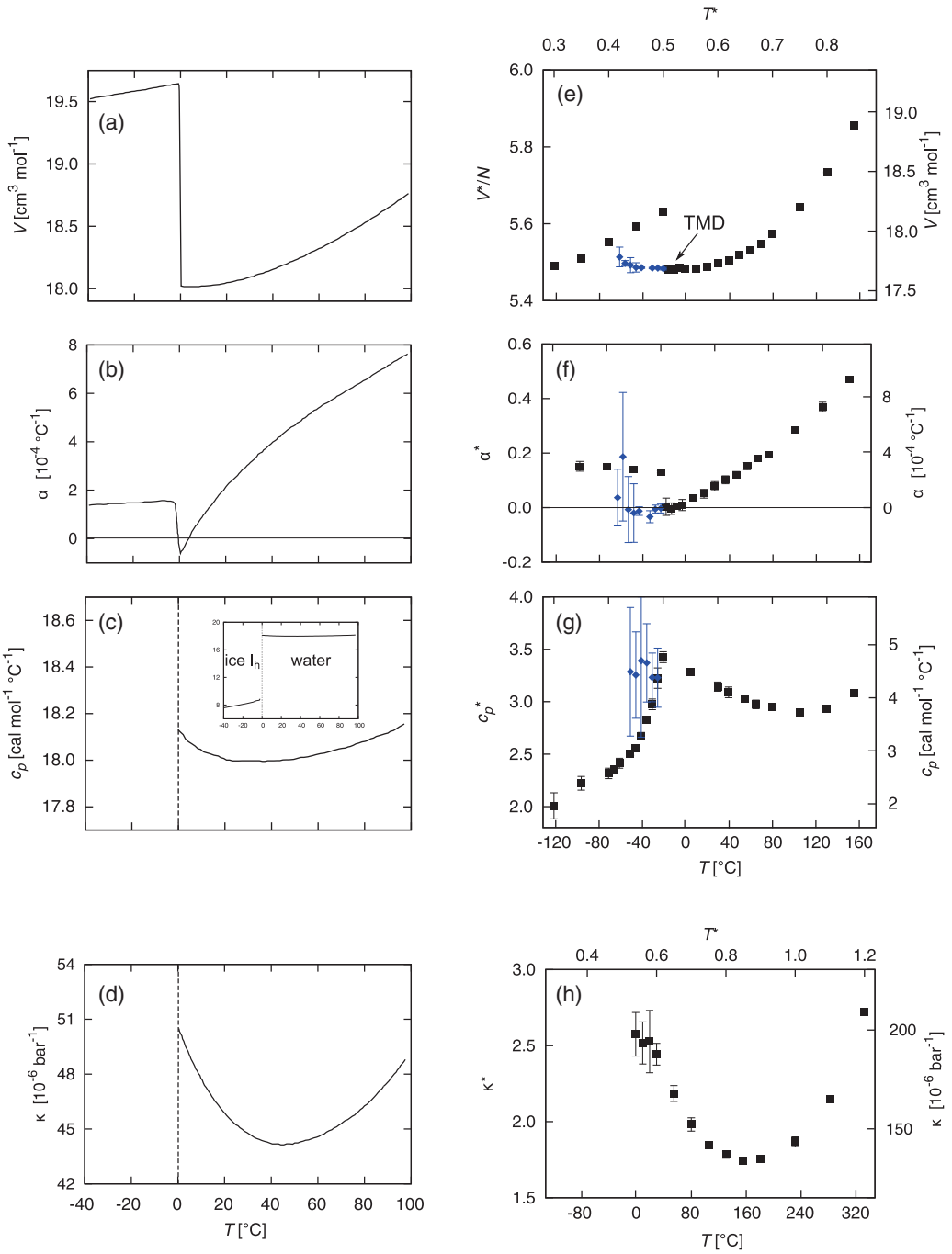


FIG. 3. (Color online) Comparison of (a)–(d) experimental data for water properties at 1 atm [1,92] and (e)–(h) simulation results of the CSW fluid at subcritical pressure, $p^* = 0.024$. The CSW model captures the appearance of the temperature of maximum density (TMD), the negative thermal expansion coefficient, and minima in the heat capacity and the isothermal compressibility. [Note a different scale and pressure $p^* = 0.10$ for (h).]

instead to see how well they can be reproduced on the sole account of having two characteristic distances, regardless of the exact slope.

Skinner *et al.* also used the x-ray diffraction technique to measure the radial distribution functions (RDFs) of liquid water at room conditions [see Fig. 2(a) for oxygen-oxygen RDF] [91]. The CSW model yields a radial distribution function at near room conditions ($T^* = 0.60$, which translates to $T = 30\,^\circ$C, and $p^* = 0.0002$ or $p = 2.6$ atm) as shown in Fig. 2(b). Even when comparing the model RDF in physical units with the experimental one, there are noticeable differences. They originate from the fact that the potential in question is an effective potential and it differs considerably. It can be seen that an unavoidable consequence of the simplicity of the model are two artifacts. First, the model introduces an additional prepeak at the position of the inner shelf in the potential, which is absent in water. This is because the model accounts for the competition between tetrahedral and trans-

lational order with the addition of the ramp in the potential. Following from this artifact is a slight underestimation of the first peak, since the model partly decouples it into the prepeak.

### C. Solvent

It is necessary that a model first correctly capture the behavior of the pure solvent if we aim to study solvation. Water has been extensively experimentally studied and the temperature dependence of its properties is well known. We used the experimental data [1,92] at 25 °C and 1 atm as a benchmark. The molar volume $V$, coefficients of thermal expansion $\alpha$, and isothermal compressibility $\kappa$, and heat capacity $c_p$ at constant pressure were compared [see Figs. 3(a)–3(d) for experimental, and Figs. 3(e)–3(h) for model data]. The simulations at a subcritical pressure ($p^* = 0.024$ or $p = 312$atm) were performed across the liquid temperature range and in the solid phase. This pressure imposed is higher than that in the experiments because the model does not show anomalies at very low pressures. Conversion of this pressure to 312 atm is an issue of parametrization and cannot be avoided; hence, we have to settle for having a subcritical pressure.

It was noted that the model manages to reproduce the anomalous trends at this higher pressure. Ice is less dense than water, which in turn displays a pronounced density maximum slightly above the freezing temperature [Figs. 3(a), 3(e)]. Between those characteristic temperatures, the thermal expansion coefficient is negative [Figs. 3(b), 3(f)]. Heat capacity of liquid water is much greater than that of ice and shows a shallow temperature-dependent minimum in the middle of the liquid temperature range (at 35 °C). Again, the model predicts a monotonic increase in the solid phase and a minimum in the liquid phase (at $T^* = 0.75$ or $T = 103$ °C) with the respect to temperature. The isothermal compressibility reaches a much more pronounced minimum at 46.5 °C in liquid water. The model features this anomaly, as well, being located at $T^* = 0.85$ or $T = 160$ °C.

We see that the liquid range of the model spans a larger area than real water. The reason for a wider liquid range (between −20 and −282 °C) is parametrization and the crudeness of the model. Also agreement between the heat capacity of model and experimental data is bad. The reason is that in our model we only have the translational component of the heat capacity. The model does not predict the rotational and vibrational contributions, which would have to be included through the dependence of the potential on the state point. This would require that all the parameters of the model be changed with respect to pressure and temperature. The model cannot be fine tuned without introducing additional parameters and constants. We opted to see how the current variation of the model performs and not to introduce further parameters. For the same reason, we do not have the correct magnitude of isothermal compressibility.

### D. Solvation and the hydrophobic effect

In the small solute limit, the hydrophobic effect is characterized as a large free energy for transfer of nonpolar solutes in water, a large negative entropy of such transfer, and strong temperature dependence of entropy and enthalpy. Consequently, it is well known [93–96] that nonpolar organic molecules exhibit a minimum in water solubility near room temperature. In other words, the free energy of transfer must

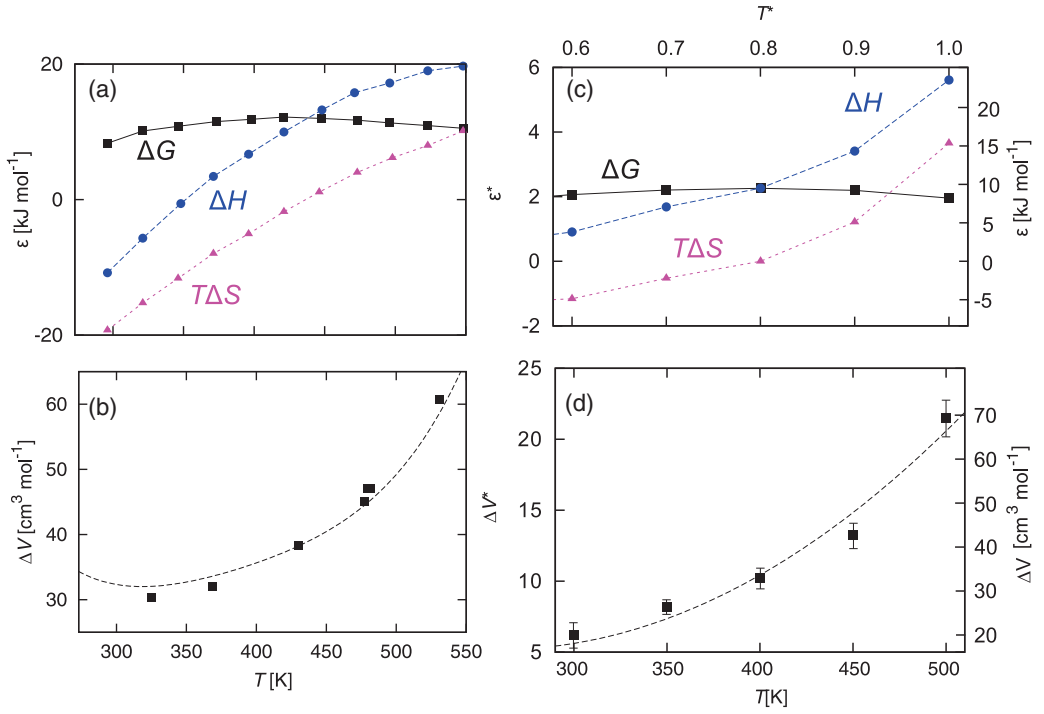


FIG. 4. (Color online) Comparison of experimental data on (a) the change of thermodynamic properties and (b) volume for transfer of argon into water at 300 atm [68,97,98] and (c)–(d) simulation results for transfer of a modified Lennard-Jones particle with $\sigma_{LJ} = 1.0$ and $\epsilon = 0.1$ into the CSW solvent at $p^* = 0.02$.

TABLE I. Established Lennard-Jones parameters for noble gases and methane in relation to water and their scaled versions for use in the CSW model.

| Molecule | Size [Å] | $\epsilon/k_b$ [K] | $\sigma^*$ | $\epsilon^*$ |
|---|---|---|---|---|
| He [100] | 2.557 | 10.22 | 0.808 | 0.013 |
| Ne [100] | 2.789 | 36.83 | 0.881 | 0.047 |
| Ar [101] | 3.404 | 116.81 | 1.075 | 0.149 |
| $CH_4$ [100] | 3.743 | 149.1 | 1.183 | 0.191 |
| Kr [102] | 3.675 | 169 | 1.161 | 0.216 |
| Xe [102] | 3.975 | 215 | 1.256 | 0.274 |
| Rn [103] | 4.35 | 290 | 1.374 | 0.371 |
| $H_2O$ [102] | 3.165 | 78.22 | 1 | 0.1 |

have a maximum. Entropy and heat capacity change of the transfer, however, show no local extrema.

We compared the experimental data for argon [68,97,98] at 25 °C and 300 atm [see Figs. 4(a)–4(b)] with our simulation trends [Figs. 4(c)–4(d)]. We modeled the argon with a modified Lennard-Jones particle with $\sigma_{LJ} = 1.0$ and $\epsilon = 0.1$. Pressure was set to $p^* = 0.02$ or 260 atm. The model also predicts a minimum in $\Delta G$ and a monotonic increase of $\Delta H$ and $T\Delta S$ with temperature. The molar volume of solute displays a minimum at low temperatures and then increases.

Checking for size dependence is somewhat more difficult. There are no real solutes that differ only in their size and have equally strong interactions with water. This is further complicated by the fact the mechanism of solvation changes as particles grow larger [99]. Noble gases and methane, however, provide an alternative way to implicitly test the size dependence. Due to the sole presence of dispersion forces, they can be described as Lennard-Jones particles. In order not to be limited just to qualitative comparison, we try to quantify the free energy of solvation for those solutes. We used the experimental LJ parameters [100–103] (see Table I). To conform them to our model, we had to scale the parameters relative to water. The Lennard-Jones size of water molecule (3.165 Å) was set to 1.0 and its attractive well ($\epsilon/k_B = 78.22$ K) was set to 0.1, attributing 90% of water-water interaction to hydrogen bonding and polar interactions, which are absent in apolar solutes. As shown in Fig. 5, the model describes the *relative* free energy of solvation for those molecules rather well. It was calculated for three different temperatures, corresponding to cold, lukewarm, and hot water ($T^* = 0.6$, 0.8, 1.0 or 30 °C, 130 °C, 230 °C). Pressure was set to the pressure where waterlike anomalies are observed (as in Fig. 3). In all three instances, the trend of solvation for different noble gases is correct, but the absolute values are off by half an order of magnitude. In cold solvent, solvation of larger solutes appears favourable, while at higher temperatures we reach the solubility minimum.

Some additional comparisons taking into account only the varying size of solutes were also done. Lum, Chandler, and Weeks (LCW) [72] developed a unified theory for solvation of apolar species of various sizes in water. We compare their results for excess chemical potential of a hard sphere in water with predictions of our model at $T^* = 1.0$ and $p^* = 0.100$. As seen in Fig. 6(a), the free energy of solvation scales quadratically with the diameter of the solute. The CSW model follows this trend. Additionally, the equivalency of different methods used (Widom's insertion technique, free energy perturbation, thermodynamic integration) is shown in Fig. 6(b). When the free energy is calculated per surface, it reaches a plateau when the solute size grows considerably larger than the solvent. As per LCW theory, this corresponds to the surface tension of pure solvent.

## V. CONCLUSION

We have shown that it is possible to obtain anomalous properties of pure solvent and solvation in the CSW model. The competition between the translational and orientational order in water manifests as two characteristic lengths in the effective potential. Therefore, using a simple potential with two characteristic lengths in simulations has turned out to be sufficient to obtain results similar to those in real water. Although direct comparison is somewhat difficult due to only two adjustable parameters the model possesses, we sought the best parametrization and cast the reduced units into physical units. Although agreement between the model and liquid water is not perfect, we have shown that it predicts the temperature of density maximum, temperature dependence of isothermal compressibility, coefficient of thermal expansion, and heat capacity. The temperature range where this happens roughly corresponds to real water.

Moreover, we have demonstrated that the quintessential hydrophobic effect can also be reproduced in such models. For small solutes, it is characterized with the temperature of

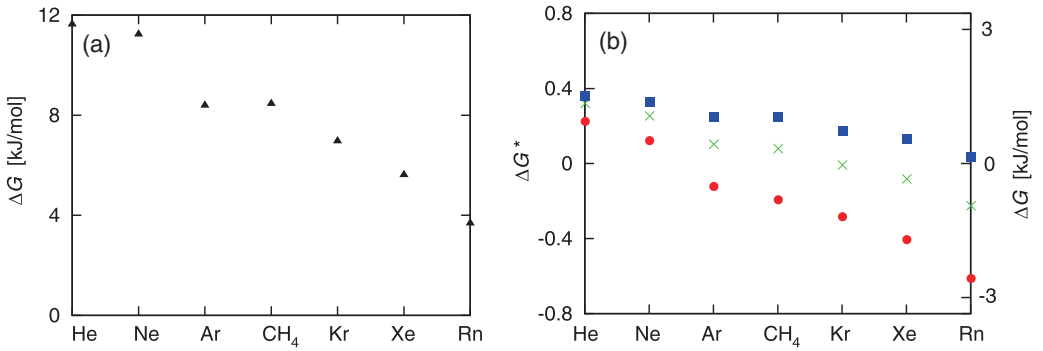


FIG. 5. (Color online) Free energy of transfer of nonpolar gases into water at 25 °C and 1 atm (left scale) [68] and results from CSW model (right) at different temperatures ($T^* = 0.6$, 0.8, 1.0) for $p^* = 0.024$. See Table I for the parameters used.

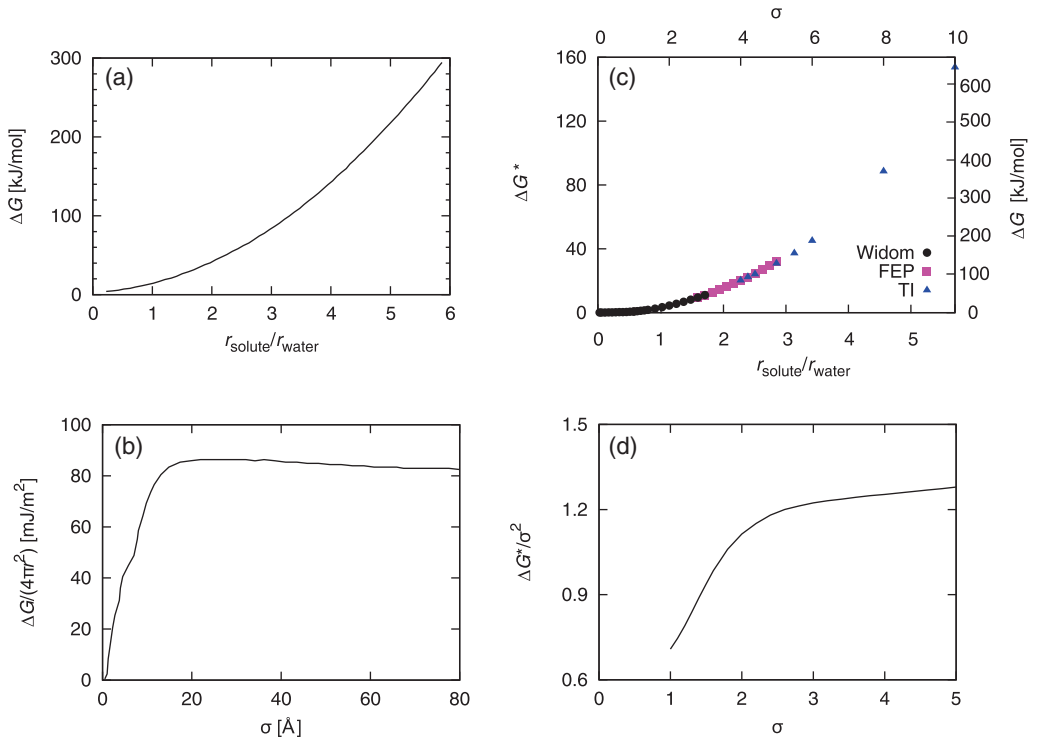


FIG. 6. (Color online) (a)–(b) Excess chemical potential for transfer of a hard sphere with radius $r$ in water [72] is in agreement with (c)–(d) the calculated trends for insertion of modified LJ solutes of various sizes in the CSW fluid at $T^* = 1.0$ and $p^* = 0.1$.

minimum solubility near room temperature, large positive heat capacity change, negative entropy at low temperatures, and high positive enthalpy at high temperatures for transfer of a nonpolar molecule into water. The CSW model predicts all these characteristics for solutes of multiple sizes. Using experimental data for noble gases interactions and conforming them to our model, we have even been able to obtain correct relative values for noble gases solvation, reproducing the trend of more favorable solvation of larger noble gases.

As previously discussed, every isotropic model introduces simplifications and artifacts, even if they are derived directly from pair correlation functions. No effort has been made to tweak the CSW model we used to the experimentally determined structural properties of water beyond the parametrization. The aim of this work was to see how many anomalies, and to what extent, could be reproduced solely on the basis of two characteristic lengths. Together with transferability issues, this constitutes the main reason for settling with the correct order of magnitude instead of futilely attempting to obtain a perfect agreement with experimental data.

## ACKNOWLEDGMENTS

We appreciate the financial support rendered by the Slovenian Research Agency (P1 0103-0201 and J1 4148), NIH (Grant No. GM063592) and the "Young Researcher" programme of Slovenia.

[1] D. Eisenberg and W. Kauzmann, *The structure and properties of water*, 1st ed. (Oxford University Press, Oxford, 1969).
[2] F. Franks and D. S. Reid, *Water. A Comprehensive Treatise*, 1st ed. (Plenum Press, New York, 1973), Vol. 2
[3] P. A. Netz, F. W. Starr, M. C. Barbosa, and H. E. Stanley, Phys. A **314**, 470 (2002).
[4] M. W. Mahoney and W. J. Jorgensen, J. Chem. Phys. **112**, 8910 (2000).
[5] M. F. Chaplin, Biochem. Mol. Biol. Educ. **29**, 54 (2001).
[6] K. A. Dill, T. M. Truskett, V. Vlachy, and B. Hribar-Lee, Annu. Rev. Biophys. Biomol. Struct. **34**, 173 (2005).
[7] P. H. Poole, F. Sciortino, U. Essman, and H. E. Stanley, Nature (London) **360**, 324 (1992).
[8] R. Sharma, S. N. Chakraborty, and C. Chakravarty, J. Chem. Phys. **125**, 204501 (2006).
[9] Y. D. Fomin, V. N. Ryzhov, and E. E. Tareyeva, Phys. Rev. E **74**, 041201 (2006).
[10] N. V. Gribova, Y. D. Fomin, D. Frenkel, and V. N. Ryzhov, Phys. Rev. E **79**, 051202 (2009).
[11] Y. D. Fomin, E. N. Tisok, and V. N. Ryzhov, J. Chem. Phys. **135**, 124512 (2011).
[12] M. S. Shell, P. G. Debenedetti, and A. Z. Panagiotopoulos, Phys. Rev. E **66**, 056703 (2002).
[13] P. H. Poole, M. Hemmati, and C. A. Angell, Phys. Rev. Lett. **79**, 2281 (1997).
[14] C. A. Angell, R. D. Bressel, M. Hemmati, E. J. Sare, and J. C. Tucker, Phys. Chem. Chem. Phys. **2**, 1559 (2000).

[15] J. W. Biddle, V. Holten, J. V. Sengers, and M. A. Anisimov, Phys. Rev. E **87**, 042302 (2013).
[16] P. H. Poole, F. Sciortino, U. Essman, and H. E. Stanley, Phys. Rev. Lett. **95**, 117802 (2005).
[17] E. G. Ponyatovskii, V. V. Sinand, and T. A. Pozdnyakova, Pis'ma Zh. Eksp. Teor. Fiz. **60**, 352 (1994) [JETP Lett. **60**, 360 (1994)].
[18] H. E. Stanley, C. A. Angell, U. E. Hemmati, M. Poole, and F. P. H. Sciortino, Physica A **205**, 122 (1994).
[19] D. A. Fuentevilla and M. A. Anisimov, Phys. Rev. Lett. **97**, 195702 (2006).
[20] A. B. de Oliveira, G. Franzese, P. A. Netz, and M. C. Barbosa, J. Chem. Phys. **128**, 064901 (2008).
[21] G. Franzese, G. Malescio, A. Skibinsky, S. V. Buldyrev, and H. E. Stanley, Nature (London) **409**, 692 (2001).
[22] H. E. Stanley and J. Teixeira, J. Phys. Chem. **73**, 3404 (1980).
[23] S. Sastry, P. G. Debenedetti, F. Sciortino, and H. E. Stanley, Phys. Rev. E **53**, 6144 (1996).
[24] R. J. Speedy, J. Phys. Chem. **86**, 982 (1982).
[25] K. Stokely, M. G. Mazza, H. E. Stanley, and G. Franzese, PNAS **107**, 1301 (2010).
[26] A. Møgelhøj, A. K. Kelkkanen, K. T. Wikfeldt, J. Shiøtz, J. J. Mortensen, L. G. M. Pettersson, B. I. Lundqvist, K. W. Jacobsen, A. Nilsson, and J. K. Nørskov, J. Phys. Chem. B **115**, 14149 (2011).
[27] F. Corsetti, E. Artacho, J. M. Soler, S. S. Alexandre, and M. V. Fernández-Serra, J. Chem. Phys. **139**, 194502 (2013).
[28] A. Ben-Naim, J. Chem. Phys. **54**, 3682 (1971).
[29] A. Bizjak, T. Urbic, V. Vlachy, and K. A. Dill, J. Chem. Phys. **131**, 194504 (2009).
[30] A. Bizjak, T. Urbič, V. Vlachy, and K. A. Dill, Acta Chim. Slov. **54**, 532 (2007).
[31] C. L. Dias, T. Ala-Nissila, M. Grant, and M. Karttunen, J. Chem. Phys. **131**, 054505 (2009).
[32] C. L. Dias, T. Hynninen, T. Ala-Nissila, A. S. Foster, and M. Karttunen, J. Chem. Phys. **134**, 065106 (2011).
[33] P. Paricaud, M. Přredota, A. A. Chialvo, and P. T. Cummings, J. Chem. Phys. **122**, 244511 (2005).
[34] F. H. Stillinger and T. A. Weber, J. Chem. Phys. **68**, 3837 (1978).
[35] G. Garde, G. Hummer, A. E. Garcia, M. E. Paulaitis, and L. R. Pratt, Phys. Rev. Lett. **77**, 4966 (1996).
[36] F. H. Stillinger and T. Head-Gordon, Phys. Rev. E **47**, 2484 (1993).
[37] T. Head-Gordon and F. H. Stillinger, J. Chem. Phys. **98**, 3313 (1993).
[38] Z. Yan, S. V. Buldyrev, N. Giovambattista, P. G. Debenedetti, and E. H. Stanley, Phys. Rev. E **73**, 051204 (2006).
[39] P. Kumar, S. V. Buldyrev, F. Sciortino, E. Zaaccarelli, and E. H. Stanley, Phys. Rev. E **72**, 021501 (2005).
[40] S. V. Buldyrev, P. Kumar, P. G. Debenedetti, P. J. Rossky, and H. E. Stanley, PNAS **104**, 20177 (2007).
[41] E. A. Jagla, J. Chem. Phys. **111**, 8980 (1999).
[42] L. Xu, S. V. Buldyrev, C. A. Angell, and H. E. Stanley, Phys. Rev. E **74**, 031108 (2006).
[43] L. Xu, N. Giovambattista, S. V. Buldyrev, P. G. Debenedetti, and H. E. Stanley, J. Chem. Phys. **134**, 064507 (2011).
[44] S. Zhou, J. Chem. Phys. **133**, 134107 (2010).
[45] A. B. de Oliveira, P. A. Netz, T. Colla, and M. C. Barbosa, J. Chem. Phys. **124**, 084505 (2006).
[46] W. P. Krekelberg, T. Kumar, J. Mittal, J. R. Errington, and T. M. Truskett, Phys. Rev. E **79**, 031203 (2009).
[47] G. Franzese, J. Mol. Liq. **136**, 267 (2007).
[48] P. C. Hemmer and G. Stell, Phys. Rev. Lett. **24**, 1284 (1970).
[49] G. Stell and P. C. Hemmer, J. Chem. Phys. **56**, 4274 (1972).
[50] E. Velasco, L. Mederos, G. Navascués, and P. C. G. S. Hemmer, Phys. Rev. Lett. **85**, 122 (2000).
[51] I. Y, S. Ono, J. Phys. F: Met. Phys. **15**, 1215 (1985).
[52] A. Voronel, I. Paperno, and S. L. E. Rabinovich, Phys. Rev. Lett. **50**, 247 (1983).
[53] P. T. Cummings and G. Stell, Mol. Phys. **43**, 1267 (1981).
[54] J. M. Kincaid and G. Stell, Phys. Lett. A **65**, 131 (1978).
[55] D. Levesque and J. J. Weis, Phys. Lett. A **60**, 473 (1977).
[56] M. Silbert and W. H. Young, Phys. Lett. A **58**, 469 (1976).
[57] K. K. Mon, N. W. Ashcroft, and G. V. Chester, Phys. Rev. B **19**, 5103 (1979).
[58] H. S. Ashbaugh and M. E. Paulaitis, J. Am. Chem. Soc. **123**, 10721 (2001).
[59] N. T. Southall and K. A. Dill, J. Phys. Chem. B **104**, 1326 (2000).
[60] M. Jochum, D. Andrienko, K. Kremer, and C. Peter, J. Chem. Phys. **137**, 064102 (2012).
[61] A. Chaimovich and M. S. Shell, Phys. Rev. E **88**, 052313 (2013).
[62] A. Chaimovich and M. S. Shell, Phys. Rev. E **89**, 022140 (2014).
[63] M. E. Johnson, T. Head-Gordon, and A. A. Louis, J. Chem. Phys. **126**, 144509 (2007).
[64] A. Chaimovich and M. S. Shell, Phys. Chem. Chem. Phys. **11**, 1901 (2009).
[65] P. Vilaseca and G. Franzese, J. Chem. Phys. **133**, 084507 (2010).
[66] P. Vilaseca and G. Franzese, J. Non-Cryst. Solids **357**, 419 (2011).
[67] M. Huš and T. Urbic, J. Chem. Phys. **139**, 114504 (2013).
[68] A. Ben-Naim, *Solvation thermodynamics*, 1st ed. (Plenum Press, New York, 1987).
[69] R. D. Cramer III, J. Am. Chem. Soc. **99**, 5408 (1977).
[70] A. Godec and F. Merzel, J. Am. Chem. Soc. **134**, 17574 (2012).
[71] C. David, Nature (London) **437**, 640 (2005).
[72] K. Lum, C. David, and J. D. Weeks, J. Phys. Chem. B **103**, 4570 (1999).
[73] M. Maiti, S. Weiner, S. V. Buldyrev, H. E. Stanley, S. Sastry, J. Chem. Phys. **136**, 044512 (2012).
[74] S. V. Buldyrev, P. Kumar, S. Sastry, H. E. Stanley, and S. Weiner, J. Phys.: Condens. Matter **22**, 284109 (2010).
[75] S. Sharma, S. K. Kumar, S. V. Buldyrev, P. G. Debenedetti, P. J. Rossky, and H. E. Stanley, Sci. Rep. **3**, 1841 (2013).
[76] C. L. Dias, T. Ala-Nissila, M. Karttunen, I. Vattulainen, and M. Grant, Phys. Rev. Lett. **100**, 118101 (2008).
[77] C. L. Dias, M. Karttunen, H. Sun Chan, Phys. Rev. E **84**, 041931 (2011).
[78] C. L. Dias, Phys. Rev. Lett. **109**, 048104 (2012).
[79] M. Huš, M. Zalar, and T. Urbic, J. Chem. Phys **138**, 224508 (2013).
[80] M. Huš and T. Urbic, J. Chem. Phys **140**, 144904 (2014).
[81] H. A. Lorentz, Annalen der Physik **248**, 127 (1881).
[82] D. Berthelot, C. R. Acad. Sci. **126**, 1703 (1898).
[83] M. P. Allen and D. J. Tildesley, *Computer Simulations of Liquids*, 1st ed. (Oxford University Press, Oxford, 1989).

[84] B. Widom, J. Chem. Phys. **39**, 2808 (1963).
[85] K. A. T. Silverstein, A. D. J. Haymet, and K. A. Dell, J. Am. Chem. Soc. **120**, 3166 (1998).
[86] R. W. Zwanzig, J. Chem. Phys. **22**, 1420 (1954).
[87] M. Huš and T. Urbic, J. Chem. Phys. **136**, 144305 (2012).
[88] B. Santra, J. Klimeš, D. Alfè, A. Tkatchenko, B. Slater, A. Michaelides, R. Car, and M. Scheffler, Phys. Rev. Lett. **107**, 185701 (2011).
[89] A. K. Soper and M. G. Phillips, Chem. Phys. **107**, 47 (1986).
[90] S. Garde and H. S. Ashbaugh, J. Chem. Phys. **115**, 977 (2001).
[91] L. B. Skinner, C. Huang, D. Schlesinger, L. G. M. Pettersson, A. Nilsson, and C. J. Benmore, J. Chem. Phys. **138**, 074506 (2013).
[92] L. D. Landau and E. M. Lifshitz, *Statistical Physics* (Butterworth-Heinemann, Oxford, 1999).
[93] R. L. Baldwin, PNAS USA **83**, 8069 (1986).
[94] S. Sawamura, K. Nagaoka, and T. Machikawa, J. Phys. Chem. B **105**, 2429 (2001).
[95] P. P. Shah, *Thermodynamics of apolar solvation in mixed aqueous solvents*, 1st ed. (ProQuest, Cambridge, 2011).
[96] M. H. Abraham, J. Am. Chem. Soc. **104**, 2085 (1982).
[97] R. Crovetto, R. Fernández-Prini, and M. L. Japas, J. Chem. Phys. **76**, 1077 (1982).
[98] D. R. Biggerstaff and R. H. Wood, J. Chem. Phys. **92**, 1988 (1988).
[99] J. R. Dowdle, S. V. Buldyrev, H. E. Stanley, P. G. Debenedeti, and P. J. Rossky, J. Chem. Phys. **138**, 064506 (2013).
[100] N. Tchouar, M. Benyettou, F. Ould Kadour, Int. J. Mol. Sci. **4**, 595 (2003).
[101] S. K. Oh, J. Thermodyn. **2013** 828620 (2013).
[102] B. Guillot, Y. Guissani, and S. Bratos, J. Chem. Phys. **95**, 3643 (1991).
[103] G. A. Miller, J. Phys. Chem. **64**, 163 (1960).